

# A numerical study of the contributions of dust source regions to the global dust budget

Taichu Y. Tanaka<sup>a,b,\*</sup>, Masaru Chiba<sup>a</sup>

<sup>a</sup> *Meteorological Research Institute, Tsukuba, Ibaraki, 305-0052, Japan*

<sup>b</sup> *JST Cooperative System for Supporting Priority Research, Japan*

Accepted 9 February 2006  
Available online 19 April 2006

## Abstract

Contributions of the nine potential dust source regions (North and South Africa, the Arabian Peninsula, Central Asia, eastern and western China, North and South America, and Australia) to the global dust budget are investigated with a global dust transport model. A six-year simulation (1990 to 1995) indicates that the greatest contributor to the global dust budget is found to be North Africa (the Sahara Desert), which accounts for 58% of the total global dust emission and 62% of the total global dust load in the atmosphere. Australian dust dominates the southern hemisphere. The dust emission and atmospheric dust load originating from East Asia (eastern and western China) are estimated to be 214 Tg yr<sup>-1</sup> and 1.1 Tg, respectively, which are 11% and 6% of the total global dust emission and dust load. Dust from East Asia dominates the atmospheric load over China and Mongolia (about 70%), Korea (60%), Japan (50%), and the North Pacific Ocean (40%). The contribution of dust originating from regions other than East Asia to the dust load over these East Asian countries and the North Pacific Ocean cannot be ignored. The simulated total dust deposition flux on Greenland suggests a possible overestimation of the Saharan dust and an underestimation of the East Asian dust in the Arctic region, which may be a common problem with global dust transport models. Possible reasons for the underestimation of the East Asian dust are discussed.

© 2006 Elsevier B.V. All rights reserved.

*Keywords:* aerosols; mineral dust; global dust model; numerical simulation; long-range dust transport

## 1. Introduction

Dust aerosol plays an important role in the climate system by affecting the radiation budget (e.g., Tegen and Lacis, 1996; Sokolik and Toon, 1996), biogeochemical cycles (Martin and Fitzwater, 1988; Martin, 1991; Archer et al., 2000), and atmospheric chemistry (Dentener et al.,

1996; Dickerson et al., 1997; Martin et al., 2003). It also affects air quality and human health (Prospero, 1999).

It is difficult to estimate the radiative effects of mineral dust since many uncertainties remain regarding the radiative properties of dust particles (Sokolik and Toon, 1996; Myhre and Stordal, 2001; Aoki et al., 2005) and the atmospheric budget for dust particles. Recent global model estimates of global dust emissions differ by more than a factor of two (ranging from 1000 to 2150 Tg yr<sup>-1</sup>); estimates of the atmospheric load differ by a factor of four (ranging from 8 to 36 Tg) (Zender et al., 2004). Tegen et al. (2002) indicated that global dust models have difficulties reproducing the magnitude of

\* Corresponding author. Meteorological Research Institute, Tsukuba, Ibaraki, 305-0052, Japan. Tel.: +81 29 853 8934; fax: +81 29 855 7240.

E-mail address: [yatanaka@mri-jma.go.jp](mailto:yatanaka@mri-jma.go.jp) (T.Y. Tanaka).

dust emissions from the Sahara and Asia. The estimated dust emissions for different source regions vary considerably among recent global models (e.g., Werner et al., 2002; Luo et al., 2003; Zender et al., 2003a; Ginoux et al., 2004; Miller et al., 2004). Dust particles from different regions have also been found to have very different optical properties (Dubovik et al., 2002; Kubilay et al., 2003). Hence, it is important to evaluate the contribution of each dust source region to reduce the uncertainties in a study of dust cycles.

Estimation of dust from East Asia is particularly difficult due to the complex topography and land-use, relatively high soil moisture, and frequent snow cover. In fact, dust concentrations in East Asia tend to be underestimated by global models (e.g., Ginoux et al., 2001; Tegen et al., 2002; Luo et al., 2003). Observational evidence implies that dust originating from East Asia has a significant influence on a global scale. For example, it is reported that East Asian dust has been transported to wide areas of the Pacific Ocean (e.g., Duce et al., 1980; Husar et al., 2001), and can reach North America (McKendry et al., 2001). Deposits of Asian dust have been identified from snow samples in Greenland (Biscaye et al., 1997; Bory et al., 2002, 2003) and even in the French Alps (Grousset et al., 2003).

Several studies have been undertaken to reproduce the global distribution of mineral dust aerosol, and regional climatologic characteristics of dust phenomena have been described in some observational studies (Pye, 1987; Goudie and Middleton, 1992). However, only a few global model studies (e.g. Luo et al., 2003) have been conducted to investigate the relative contribution of dust source regions and to reproduce the regional characteristics of dust source regions. We performed a numerical experiment in this study using a global dust transport

model that treats dust aerosol from different source regions separately. We describe the global aerosol transport model and the dust emission scheme in Section 2. We present the results of the numerical simulation and discuss the contribution of each source region in Section 3. Emphasis is given to the budget and the contribution of East Asian dust. We will also examine the contributions to the dust deposition on Greenland to determine whether the East Asian influence over the area is dominant. Section 4 presents the conclusions of this study.

## 2. Model description

### 2.1. Model framework

We used the Model of Aerosol Species IN the Global Atmosphere (MASINGAR), which is a chemical transport model (CTM) for tropospheric aerosol species (Tanaka et al., 2003; Tanaka and Chiba, 2005). This CTM is on-line coupled with a general circulation model (GCM) called MRI/JMA 98 GCM (Shibata et al., 1999), which includes direct radiation feedback of dust aerosol. However, the direct radiation feedback calculation of dust was not applied in this simulation since we chose to investigate the transport of dust with assimilated meteorological conditions. MASINGAR simulates mineral dust, nss-sulfate, carbonaceous, and sea-salt aerosols. This model is also used by the Japan Meteorological Agency for operational dust forecasting.

The atmospheric transport was calculated using a semi-Lagrangian advection scheme and schemes for sub-grid turbulent vertical diffusion and convective transport. The eddy diffusivity for vertical diffusion was calculated using the level-2 turbulence closure scheme of Mellor and Yamada (1974). The convective transport was calculated

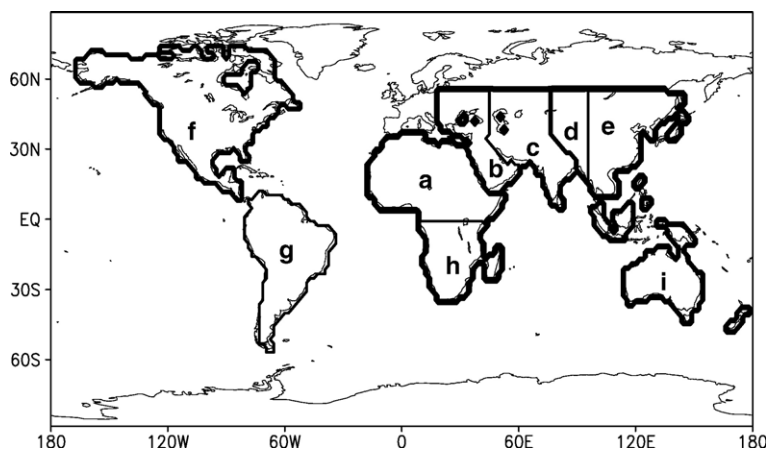


Fig. 1. Borders of the dust source regions. (a) North Africa, (b) Arabian Peninsula, (c) Central Asia, (d) Western China, (e) Eastern China, (f) North America, (g) South America, (h) South Africa, (i) Australia.

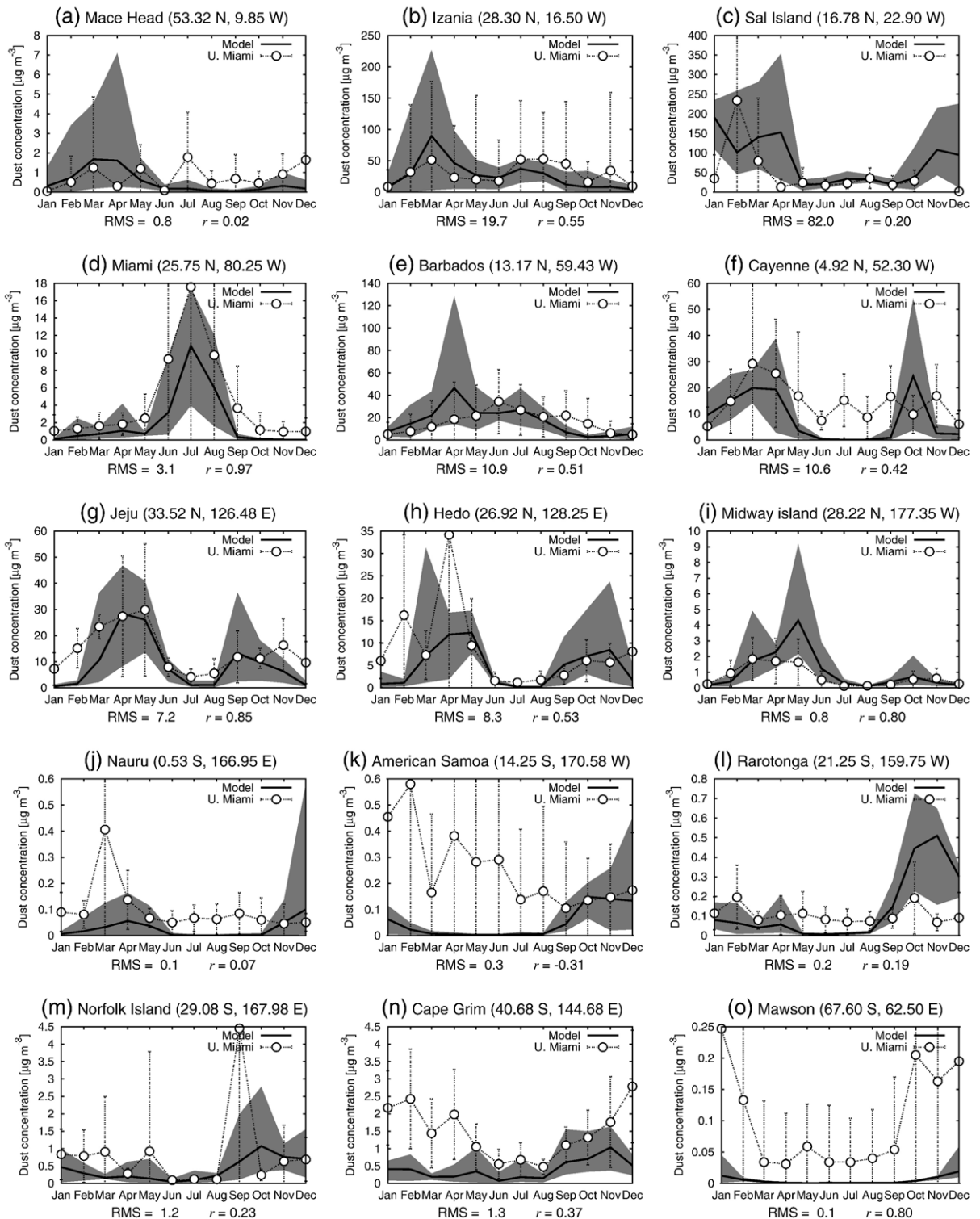


Fig. 2. Comparison of the observed (circles with dash) and simulated (solid lines) monthly mean surface dust concentration at the sites of the University of Miami aerosol network (unit:  $\mu\text{g m}^{-3}$ ). Maximum and minimum values of a six-year simulation are represented by shading for the simulated values. One standard deviation is indicated by whiskers for the observed values.

using the updraft mass flux of the Arakawa–Schubert moist convection scheme (Arakawa and Schubert, 1974) as in the MRI/JMA 98 GCM. Dry deposition was parameterized with the resistance-in-series model (Seinfeld and Pandis, 1997), which includes turbulent impaction and gravitational settling. In-cloud scavenging was calculated using the scheme of Giorgi and Chameides (1986), and below-cloud scavenging was calculated based on the theory of Seinfeld and Pandis (1997). Both the dry and wet deposition schemes were particle-size dependent. The model resolutions are variable. In this study, those were set to a T63 Gaussian horizontal grid (about  $1.8^\circ \times 1.8^\circ$ ) and 30 vertical layers in the hybrid  $\sigma$ - $p$  vertical coordinate from the surface to a height of 0.8 hPa. The model has a built-in four-dimensional data assimilation system with a nudging scheme, which enables the model to perform a realistic simulation of a specific period.

The dust aerosol was divided into ten size-classes from 0.2 to 20  $\mu\text{m}$  in diameter, which were transported independently and assumed to be non-interacting. This model calculates the dust emission flux based on the saltation-bombardment theory, and source areas are determined by vegetation cover, snow cover, land-use type, and soil type. Tanaka and Chiba (2005) gave a more detailed description of the treatment of dust aerosol and validation with available observations; Tanaka et al. (2005) used this model in a case study of long-range transport of a dust storm event. We describe our calculation of dust emission below.

### 2.2. Calculation of dust emission

The mobilization of soil particles is initiated when the friction velocity on a bare surface ( $u_{*s}$ ) exceeds a threshold value called the threshold friction velocity ( $u_{*t}$ ), which is calculated using the formula of Shao and Lu (2000) with the soil moisture factor ( $f_w$ ) of Fécán et al. (1999), as

$$u_{*t}(D) = f_w \sqrt{A_N \left( \frac{\rho_p g D}{\rho_a} + \frac{\Gamma}{\rho_a D} \right)}, \quad (1)$$

where  $D$  is the particle diameter,  $g$  is the gravitational acceleration,  $\rho_a$  is the air density,  $\rho_p$  is the particle density,  $A_N = 0.0123$ , and  $\Gamma = 3 \times 10^{-4} \text{ kg s}^{-2}$ . The soil moisture factor  $f_w$  is calculated by

$$f_w = \begin{cases} 1 & w \leq w_r \\ \sqrt{1 + a[100(w - w_r)]^b} & w > w_r \end{cases} \quad (2)$$

where  $w$  is the gravimetric soil water content and  $w_r$  is the threshold gravimetric soil water content. The em-

pirical constants  $a$  and  $b$  were set to  $a=1.21$  and  $b=0.68$ . We again followed the parameterization of Fécán et al. (1999) to calculate  $w_r$ ,

$$w_r = 0.17M_{\text{clay}} + 0.14M_{\text{clay}}^2, \quad (3)$$

where  $M_{\text{clay}}$  is the mass fraction of clay in the soil.  $M_{\text{clay}}$  was taken from the global soil texture database of Webb et al. (2000).

The dust flux in the size range  $[D_i, D_{i+1}]$  was calculated based on the theory of Shao et al. (1996);

$$\Delta F_{i0} = CA \frac{2\rho_p\gamma}{3\rho_a} \int_{D_i}^{D_{i+1}} \frac{\beta_2(D_d)}{u_{*t}(D_d)^2} p(D_d) dD_d \times \int_0^\infty \beta_1(D_s) \hat{Q}(D_s) p(D_s) dD_s \quad (4)$$

where  $D_d$  is the diameter of emitted dust particles,  $D_s$  is the diameter of saltating particles,  $\hat{Q}(D_s)$  is the mass flux of saltating particles,  $p(D)$  is the size distribution of the parent soil,  $A$  is the erodible areal fraction of the model grid, and  $C (= 1 \times 10^{-3})$  is a global tuning factor that was chosen to yield an annual global source strength of about  $2100 \text{ Tg yr}^{-1}$  (Penner et al., 2001) in a 25-year simulation in a previous study (Tanaka and Chiba, 2005).

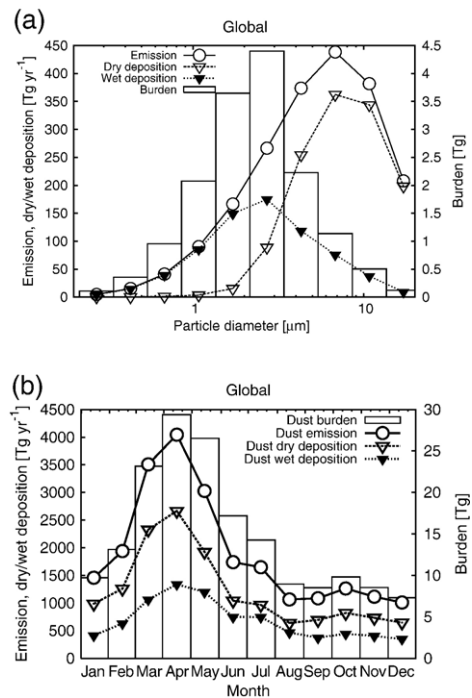


Fig. 3. Annually and globally averaged dust emission flux, dry and wet deposition flux, and atmospheric load. (a) Size dependence. (b) Seasonal variation.

Following Shao et al. (1996),  $\gamma \sim 2.5$  and  $\beta_1$  and  $\beta_2$  appear as functions of  $D_s$  and  $D_d$ ,

$$\beta_1(D_s) = 0.125 \times 10^{-4} \ln(D_s) + 0.328 \times 10^{-4} \quad (5)$$

$$\beta_2(D_d) = \exp(-140.7D_d + 0.37). \quad (6)$$

The saltation flux  $\tilde{Q}(D_s)$  is calculated using a formula from Owen (1964)

$$\tilde{Q}(D_s) = \begin{cases} \frac{c_s(D_s)\rho_a u_{*s}^3}{g} \left( \frac{1 - u_{*t}(D_s)^2}{u_{*s}^2} \right) & u_{*s} > u_{*t} \\ 0 & u_{*s} \leq u_{*t} \end{cases} \quad (7)$$

where

$$c_s(D_s) = 0.25 + \frac{V_s(D_s)}{3u_{*s}}, \quad (8)$$

where  $V_s(D_s)$  is the gravitational settling velocity of a saltating particle with diameter  $D_s$ .

We specified the size distribution of the parent soil using the global soil texture database of Webb et al. (2000). This database has a horizontal resolution of  $1^\circ \times 1^\circ$  and 15 soil horizons, and specifies the percentage of sand ( $D \geq 50 \mu\text{m}$ ), silt ( $2 < D < 50 \mu\text{m}$ ), and clay ( $D \leq 2 \mu\text{m}$ ) for individual soil horizons. We used data from the uppermost soil horizon, since the conditions for dust emission generally occur only at the surface.

We assumed that the distribution could be expressed by a tri-modal lognormal probability density function, which is similar to the method used by Lunt and Valdes (2002). The soil particle-size distribution is expressed as

$$\frac{dM(D)}{d\log D} = \sum \frac{M_i}{\sqrt{2\pi}\sigma_i} \exp\left(\frac{-(\log(D/\tilde{D}_i))^2}{2\sigma_i^2}\right), \quad (9)$$

where mode  $i$  is for sand, silt, or clay.  $M_i$  is the mass fraction of the  $i$ -th mode, taken from the database of

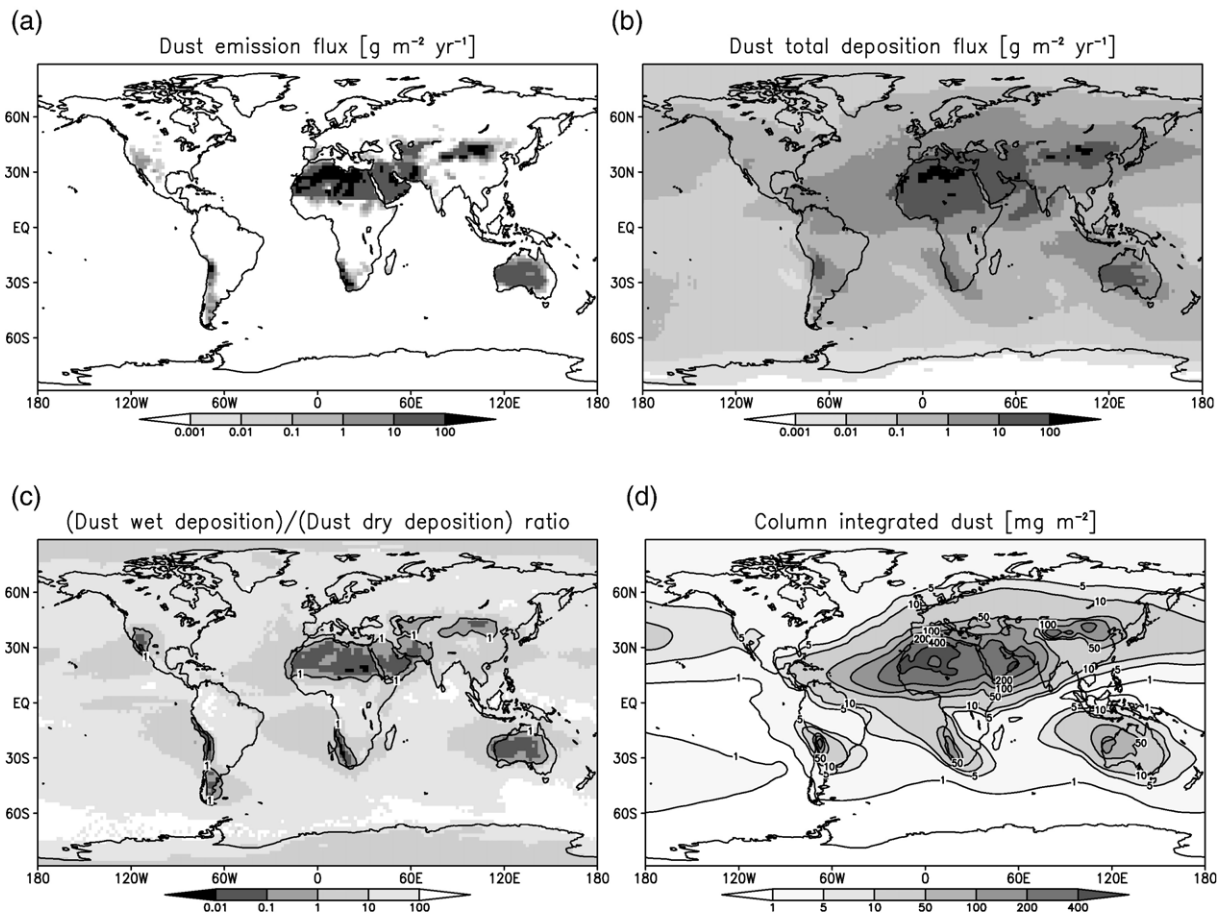


Fig. 4. Simulated annually averaged (a) dust emission flux, (b) total deposition flux, (c) ratio of wet deposition to dry deposition, and (d) atmospheric load.

Webb et al. (2000). The parameters  $\tilde{D}_i$  and  $\sigma_i$  were set to  $\tilde{D}_{\text{sand}}=300 \mu\text{m}$ ,  $\tilde{D}_{\text{silt}}=10 \mu\text{m}$ ,  $\tilde{D}_{\text{clay}}=1.6 \mu\text{m}$ ,  $\sigma_{\text{sand}}=0.8$ ,  $\sigma_{\text{silt}}=1.0$ , and  $\sigma_{\text{clay}}=1.0$ , which are slightly modified from the parameters used in Tanaka and Chiba (2005) since comparisons between simulated dust size distributions by the previous model and the retrieval calculations based on observation by the sun-photometers suggested that the model produces too much clay fraction (T. Aoki, personal communication). The mode diameter  $\tilde{D}_i$  was determined to be a representative size for each mode. We chose the geometric standard deviation  $\sigma_i$  to be large enough that the three modes were connected continuously, but small enough that there would not be too much overlap of the modes and so the resulting distributions would be similar to the measured particle-size distributions (e.g., Shao, 2000). This determination is somewhat subjective, and we are planning a sensitivity study of these parameters to evaluate their uncertainties. We have not included the effect of the changes of the soil particle-size distribution under disturbed soil conditions (Shao, 2000), since there is very little quantitative information available on a global scale.

The erodible areal fraction  $A$  is expressed by the following factorial form:

$$A = (1-A_v)(1-A_s)(1-A_w)A_lA_t, \quad (10)$$

where  $A_v$ ,  $A_s$ ,  $A_w$ ,  $A_l$ , and  $A_t$  represent the factors of vegetation cover, snow cover, water cover, land-use type, and soil type. The factor of vegetation cover  $A_v$  was calculated as a function of the leaf area index (LAI), which was calculated by the land surface model in the MRI/JMA 98 GCM, which uses a monthly mean LAI database from Wilson and Henderson-Sellers (1985). The snow cover fraction was prognostically calculated by the land surface model.  $A_w$  is the fraction of water in

the grid-box and was calculated using the U.S. Geological Survey (USGS; <http://info.er.usgs.gov>) database. Factor  $A_l$  was set to zero where the land-use type is broadleaf or coniferous evergreen forest in the database of DeFries and Townshend (1994); it was otherwise set to unity. Factor  $A_t$  was set to zero with the soil-type “lithosol” in the database of Zobler (1986); it was otherwise set to unity.

There are other factors that must be considered for dust emission. Many recent global models use the “hot spots” parameterization to account for the observed fact that the regions where the Total Ozone Mapping Spectrometer (TOMS) aerosol index climatologically corresponds strongly to the topographic depression, since fine dust sediments are accumulated in those areas (e.g., Ginoux et al., 2001; Prospero et al., 2002; Tegen et al., 2002; Zender et al., 2003b). The introduction of the “hot spot” parameterization may improve calculations of dust emissions in topographic depression areas such as the Taklimakan desert, Australia, or Lake Chad. However, our current model does not explicitly treat the “hot spots” parameterization, since our model incorporates the effect of soil texture into the calculation of dust emission flux. Fine dust deposits accumulated in a topographic depression should be reflected in the soil texture database, although the soil texture databases used in the present model were constructed for agricultural purposes and may not be suitable for calculating dust emission flux.

### 2.3. Apportionment of the source regions

The land area was divided into nine potential dust source regions, as suggested by Prospero et al. (2002), i.e., North and South Africa, the Arabian Peninsula, Central Asia, eastern and western China, North and South America, and Australia, to identify the relative

Table 1

Annual dust budget from each source region. Numbers in the parentheses in the dry and wet deposition columns are the percentages for each deposition to the total deposition. The different lifetimes in this table are defined as follows: Dry lifetime = (Dust load)/(Dry deposition), Wet lifetime = (Dust load)/(Wet deposition), and Total lifetime = (Dust load)/(Dry deposition + Wet deposition)

	Emission (Tg yr <sup>-1</sup> )	Dry deposition (Tg yr <sup>-1</sup> )	Wet deposition (Tg yr <sup>-1</sup> )	Burden (Tg)	Dry lifetime (days)	Wet lifetime (days)	Total lifetime (days)
North Africa	1087	723 (67%)	363 (33%)	9.09	4.6	9.1	3.1
Arabian Peninsula	221	129 (58%)	92 (42%)	1.65	4.7	6.6	2.7
Central Asia	140	94 (67%)	46 (33%)	1.05	4.1	8.3	2.7
Western China	68	39 (57%)	29 (43%)	0.42	3.9	5.2	2.2
Eastern China	146	90 (62%)	56 (38%)	0.67	2.7	4.3	1.7
North America	2	1 (59%)	1 (41%)	0.01	3.9	5.5	2.3
South America	44	20 (45%)	24 (55%)	0.30	5.5	4.6	2.5
South Africa	63	41 (64%)	23 (36%)	0.47	4.2	7.6	2.7
Australia	106	65 (61%)	41 (39%)	0.92	5.2	8.2	3.2
Total	1877	1202 (64%)	675 (36%)	14.6	4.4	7.9	2.8

contributions of mineral dust from different source regions to the global dust budget. The borders of the source regions are designated in Fig. 1. Dust fluxes from different source regions were assigned to separate tracers and transported independently. This treatment enables us to evaluate dust emission, concentration, and deposition for each source region independently, although it requires many more computational resources than a normal simulation.

### 3. Results and discussion

We performed a simulation for the six-year period from 1990 to 1995. One-month spin-up integra-

tion from a zero dust concentration was conducted before the simulation to generate the initial dust field. The results were stored as daily and monthly mean values. The horizontal wind components were assimilated with the six-hourly data of the reanalysis of the National Centers for Environmental Prediction–Department of Energy Atmospheric Model Intercomparison Project (NCEP–DOE AMIP-II) (Kanamitsu et al., 2002) to obtain a realistic atmospheric field. The sea surface temperature and ice data were prescribed by the monthly mean HadISST v1.1 data (The British Atmospheric Data Centre, <http://badc.nerc.ac.uk/data/hadisst/>) for the corresponding years.

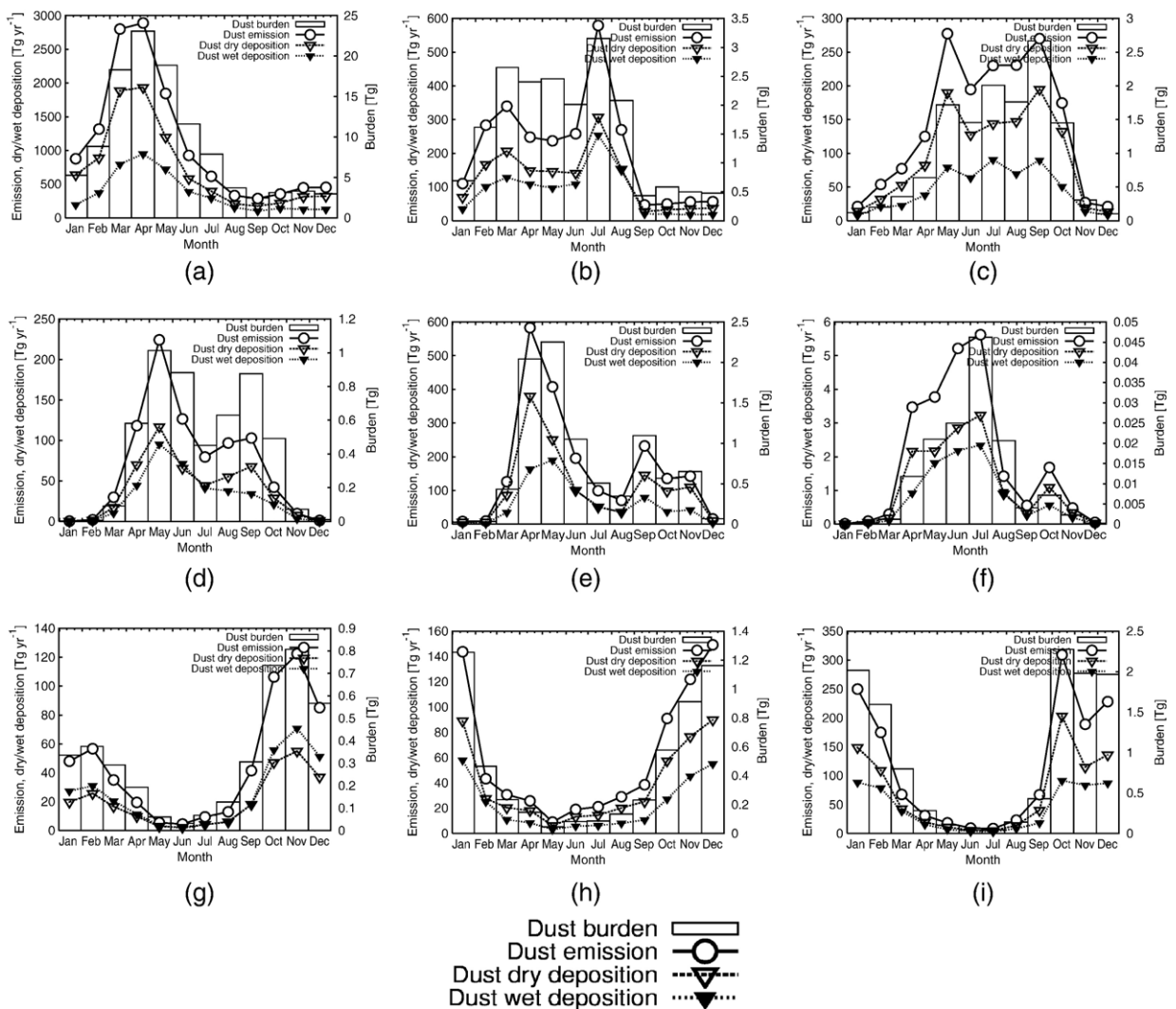


Fig. 5. Simulated monthly averaged dust emission flux, dry deposition flux, wet deposition flux, and atmospheric load for each source region. (a) North Africa, (b) Arabian Peninsula, (c) Central Asia, (d) Western China, (e) Eastern China, (f) North America, (g) South America, (h) South Africa, (i) Australia.

### 3.1. Global distribution of simulated dust

We present here a comparison of the simulated and observed monthly mean dust concentrations. Fig. 2

compares the simulated monthly mean surface dust concentration with that of the University of Miami aerosol network data (J. Prospero and D. Savoie, personal communication). The dataset consists of monthly

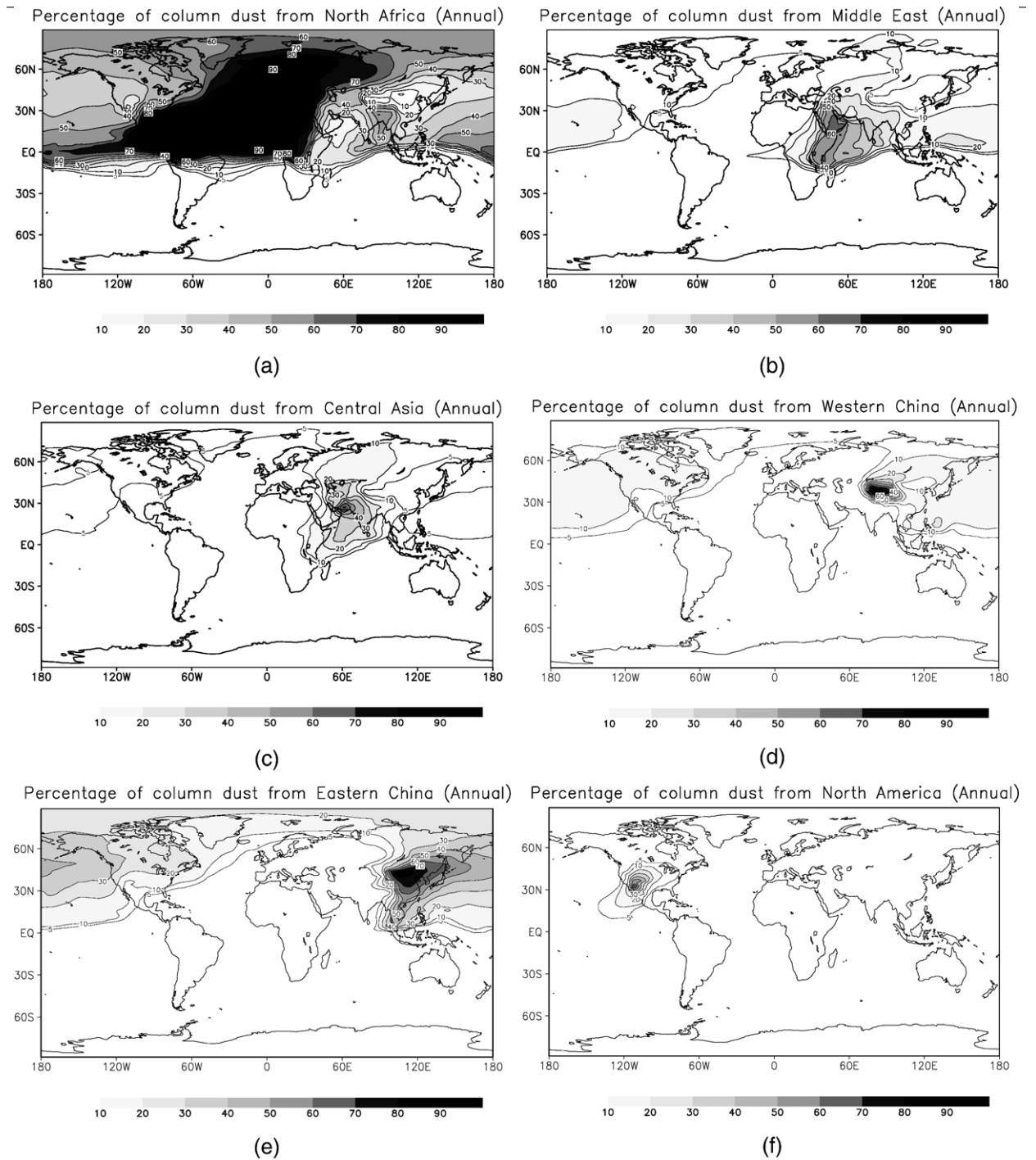


Fig. 6. Relative contributions (in percentage) of the annually averaged column integrated dust mass from each source region. (a) North Africa, (b) Arabian Peninsula, (c) Central Asia, (d) Western China, (e) Eastern China, (f) North America, (g) South America, (h) South Africa, (i) Australia.

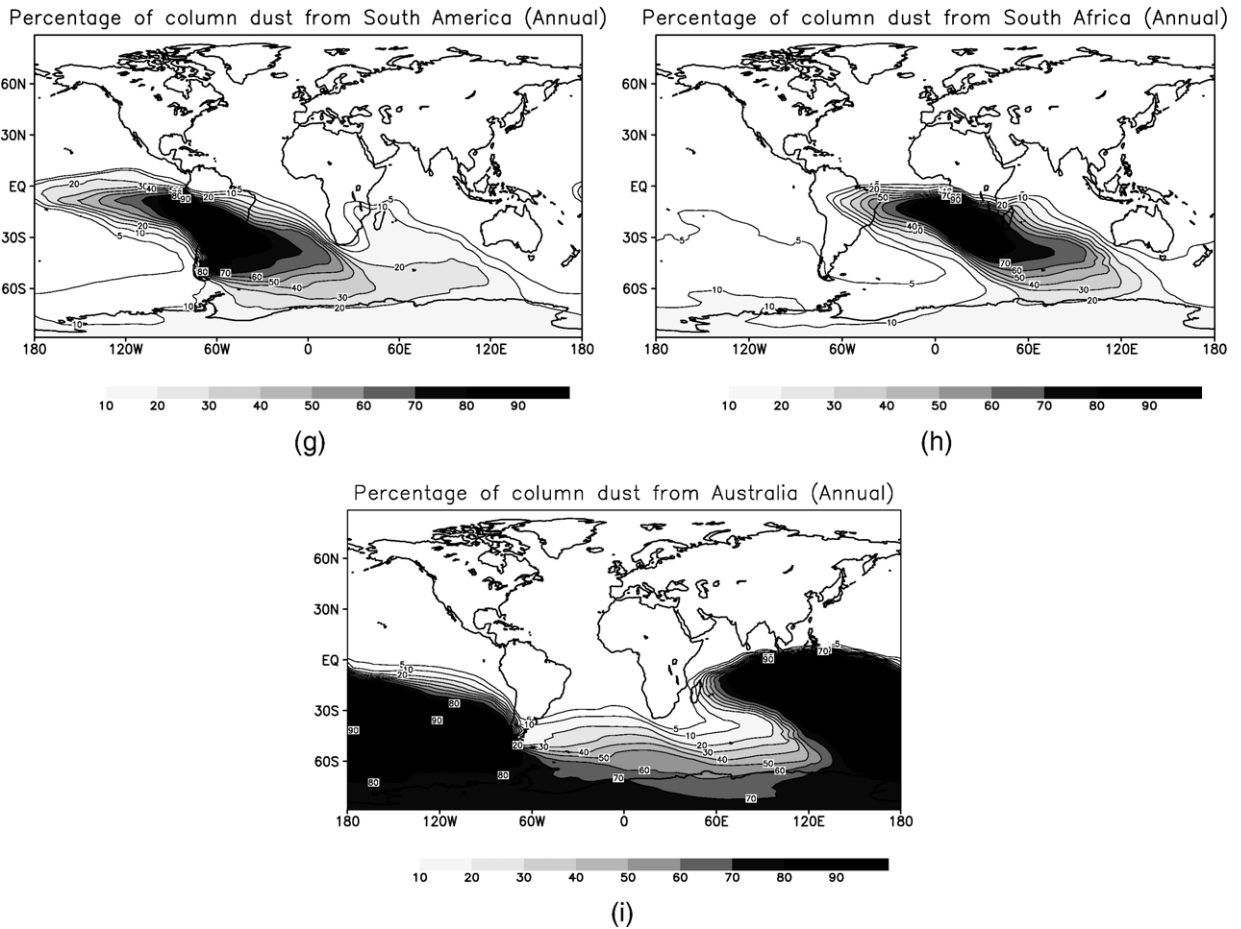


Fig. 6 (continued).

records of surface dust concentration measurements, taken primarily at remote locations. Seasonal variations of dust concentrations at stations in the northern hemisphere are generally well simulated, although some disagreements can be found. Two stations near the East Asian dust source regions (Fig. 2g and h) reveal good correlations, with a primary peak in spring and a secondary peak in autumn. The results of the stations near and downwind of the Sahara suggest that this model tends to overestimate the spring dust and underestimate the summer and autumn dust from the Saharan region. Dust concentrations at the stations in the southern hemisphere tend to be underestimated, particularly in Antarctica (Fig. 2o).

We will now examine the simulated global budget and distribution of dust from all source regions. Fig. 3a depicts the annually and globally averaged global dust-emission fluxes, the dry and wet deposition fluxes, and the dust load for each size-bin. The annual and global dust-emission fluxes and the lifetime of this simulation

are  $1877 \text{ Tg yr}^{-1}$  and 2.8 days. Fig. 3a indicates that the dust-emission flux has its peak around  $7 \mu\text{m}$ , but the atmospheric dust load has a peak around 2 to  $3 \mu\text{m}$ . The dry deposition flux is dominated by the silt particles (diameter  $> 2 \mu\text{m}$ ) due to the large gravitational settling velocity. In contrast, clay particles (diameter  $\leq 2 \mu\text{m}$ ) are mainly scavenged by wet deposition. However, sensitivity experiments are required to draw solid conclusions since there are uncertainties in the determination of the parent soil size distributions.

Fig. 3b illustrates the seasonal variations of the dust emission, deposition, and load. The global total dust emission and the corresponding deposition and load were greatest during the spring of the northern hemisphere.

The annual mean global distributions of dust emissions, dry and wet depositions, and column integrated dust masses are depicted in Fig. 4a–d. Fig. 4a demonstrates that the major dust source regions correspond to bare desert and semi-desert regions. Fig. 4b indicates

that high dry deposition flux occurs in the source regions because of the sedimentation of large particles. In contrast, high wet deposition flux occurs far from the dust source regions (Fig. 4c). High wet deposition flux occurs over the tropical Atlantic and Indian Oceans since wet deposition flux is associated not only with the dust concentration but also with precipitation.

The annual mean simulated column dust amount is presented in Fig. 4d. The peak values of column dust masses were located over North Africa, the Arabian Peninsula, the Chinese deserts (i.e., the Taklimakan and the Gobi deserts), Australia, South Africa, Chile (the Atacama desert), and Patagonia. Our column dust mass patterns are similar to those in previous global dust model studies (Ginoux et al., 2001; Tegen et al., 2002;

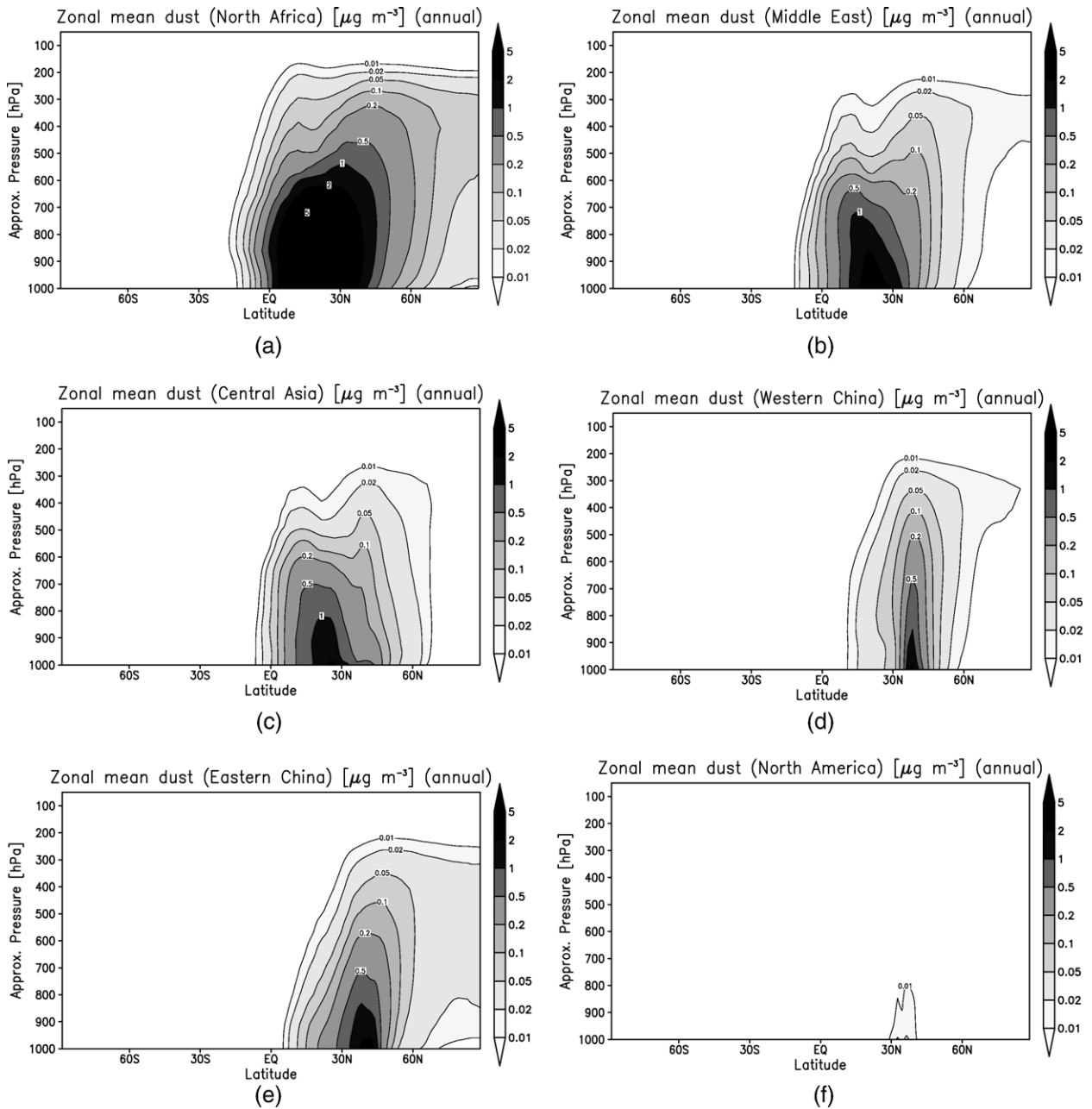


Fig. 7. Annually averaged zonal mean distribution of dust from each source region in  $\mu\text{g m}^{-3}$ . (a) North Africa, (b) Arabian Peninsula, (c) Central Asia, (d) Western China, (e) Eastern China, (f) North America, (g) South America, (h) South Africa, (i) Australia.

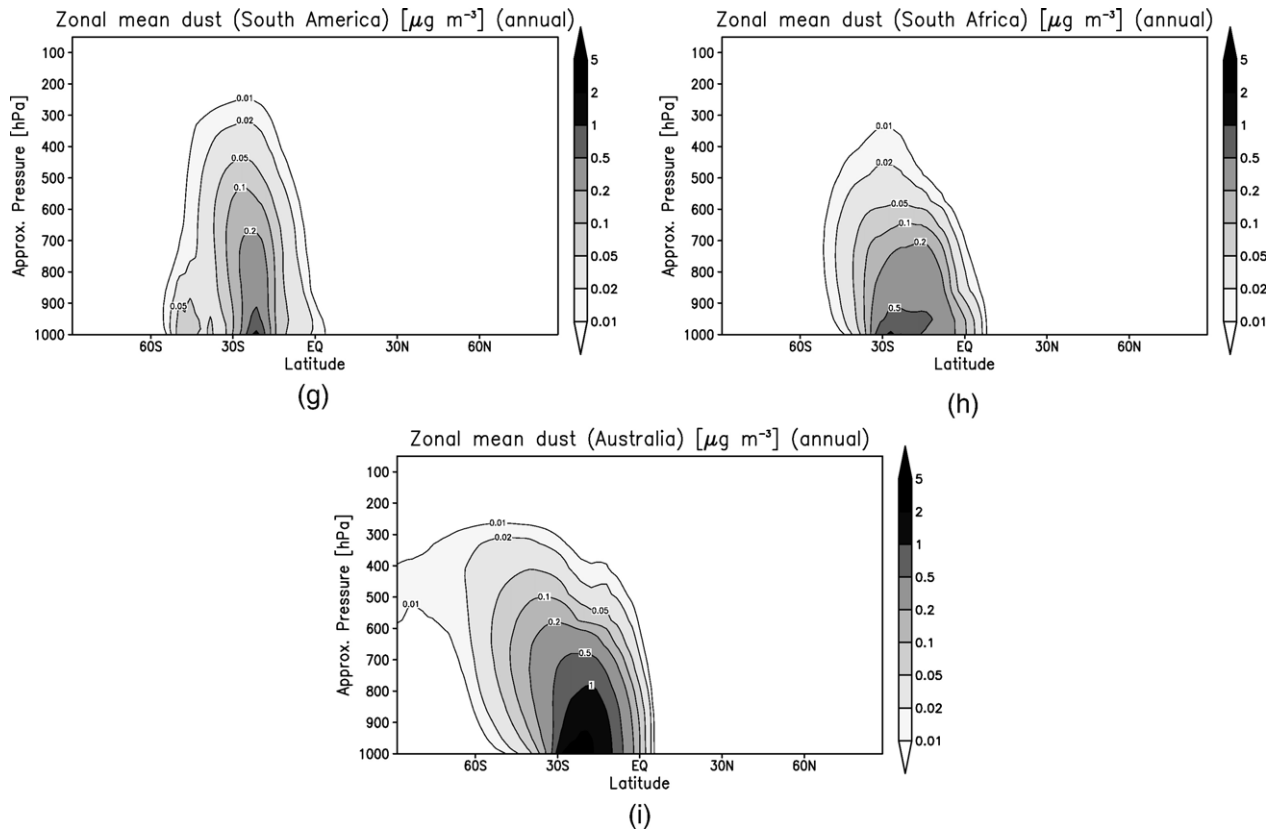


Fig. 7 (continued).

Lunt and Valdes, 2002; Zender et al., 2003a; Miller et al., 2004). However, the peaks over the East Asian region were higher than those of previous studies. Our results reveal a large peak over Chile and South Africa, whereas some models (Tegen et al., 2002; Zender et al., 2003a) do not. The maximum over Australia was located in the western area, although the maximum was seen over Lake Eyre in some models and in the TOMS aerosol index (Prospero et al., 2002).

### 3.2. Dust mass budget of each source areas

The annual means of total dust emission, atmospheric load and lifetime for different source areas are listed in Table 1. The most important dust source area was North Africa, with about 58% of the global total dust emission and 62% of the global total atmospheric dust load. Luo et al. (2003) reported a similar result with a greater contribution from North Africa than in this study, accounting for 67% of the total dust emission and 73% of the total dust load. Australia exhibited the greatest contribution of dust in the southern hemisphere, ac-

counting for 5.6% of the total dust emission and 6.3% of the total dust load. The emission flux and atmospheric load of dust from East Asia were  $214 \text{ Tg yr}^{-1}$  and  $1.1 \text{ Tg}$ , which represent 11% and 6% of the total emission and load. Specifically, the western China (the Taklimakan desert) origin was  $0.4 \text{ Tg}$ , and the eastern China (the Gobi desert) origin was  $0.7 \text{ Tg}$ .

The lifetime of dust from different regions varies from 1.7 to 3.2 days. Both dry and wet deposition lifetimes vary from region to region, due to the difference in transport and precipitation. Dust from eastern China (the Gobi desert) has the shortest lifetime (1.7 days). Luo et al. (2003) also described the short lifetime of East Asian dust due to the relatively high precipitation frequency in East Asia.

Fig. 5 presents the seasonal variation of emissions, depositions and atmospheric loads of dust from different regions. The dust budget has different seasonal characteristics in different regions. Dust emission was generally small in the winter season in all dust source regions. The seasonal variation of North African dust (Fig. 5a) displayed a pattern similar to that of the total global dust

(Fig. 3b), which indicates that the global dust budget is strongly controlled by the North African dust budget. Most of the regions exhibited substantial dust emission from spring to autumn. However, dust from eastern China (the Gobi desert) revealed a primary peak in spring and secondary peak in autumn and decreased in summer (Fig. 5e). The cause of this seasonal variation is that the extratropical cyclones are active in spring and autumn, while vegetation growth and elevated soil moisture content (due to precipitation) over the region during the summer season prevent dust emission. The observed seasonal variation of dust phenomena in East Asia also revealed a primary peak in spring and a secondary peak in autumn (Kurosaki and Mikami, 2005).

### 3.3. Dust distribution and contribution from different source regions

Fig. 6 presents the percentages of annual mean column dust from the source regions. The simulated results indicate that North African dust prevails over a wide area of the northern hemisphere (Fig. 6a). It dominates not only over the northern part of the Atlantic but also the northern hemisphere. Dust from the Arabian Peninsula and Central Asia is primarily transported southward, and has a significant influence over the Indian Ocean (Fig. 6b and c). Fig. 6d and e indicates that dust from East Asia (eastern and western China) spreads eastward over the northern Pacific Ocean (over 40%) and northward to the Arctic region (about 30%). Dust from North America is minimal and localized (Fig. 6f). Australian dust dominates over the southern Pacific Ocean and the Antarctica in the southern hemisphere (Fig. 6i).

Dust from eastern and western China dominates the atmospheric dust load over East Asia; about 70% over China and Mongolia, 60% over the Korean Peninsula, and 50% over Japan. However, the simulated result indicates that dust from other source regions such as

North Africa and the Arabian Peninsula, also contributes to the dust load over East Asia. An annual average of over 20% to 30% of the dust load over East Asia is attributed to Saharan dust and up to 10% to Arabian dust. This is partly due to seasonal variations of the dust emissions; the Sahara desert emits dust throughout the year, whereas dust emission from East Asia almost ceases in winter. However, comparisons with the observed surface dust concentrations suggest that the contribution of Saharan dust to East Asia may be overestimated in our model. Nevertheless, cases of possible dust transport from the Sahara and the Middle East to East Asia have been reported (Tazaki et al., 2004; Tanaka et al., 2005; Park et al., 2005) and the influence of dust from regions other than China and Mongolia on East Asia cannot be ignored.

Fig. 7 illustrates the zonal mean distribution of dust from each source region. The dust concentration generally decreases rapidly with height over the dust source regions. The dust concentration is greater at an increased altitude at high latitudes ( $>60^\circ$ ) as a result of the poleward dust transport at high altitudes. North African dust makes the greatest contribution to the northern hemisphere, as expected from the horizontal distribution. The figure indicates that East Asian dust is transported to a high latitude, while dust from the Arabian Peninsula and Central Asia tends to be transported equatorward. Dust over Antarctica is dominated by Australian dust, which has a peak around 500 hPa in altitude.

The results indicate that dust originating from East Asia (western and eastern Asia) exerts relatively significant influence over the Arctic region. Dust over the high latitudes may have significantly impact climatic changes due to its radiative effect and deposition over snow and ice. Radiative forcing of dust aerosol over high latitude tends to be positive due to the highly visible albedo of the underlying snow surface. Snow impurities originating from the deposition of atmospheric aerosol are considered to be the main cause of

Table 2

Comparison of the regional annual mean dust flux between this study and other recent studies of global dust models. The unit is  $\text{Tg yr}^{-1}$ . Numbers in parentheses are the percentages for the annual mean global emission flux

	Africa		Asia			America		Australia	Global
	North	South	Arabia	Central	East	North	South		
This study	1087 (57.9%)	63 (3.4%)	221 (11.8%)	140 (7.5%)	214 (11.4%)	2 (0.1%)	44 (2.3%)	106 (5.7%)	1877
Werner et al. (2002)	693 (65%)		101 (9.5%)	96 (9.0%)				52 (4.9%)	1060
Luo et al. (2003)	1114 (67%)		119 (7.2%)		54 (3.2%)			132 (8.0%)	1654
Zender et al. (2003a)	980 (66%)		415 (28%)			8 (0.5%)	35 (2.3%)	37 (2.5%)	1490
Ginoux et al. (2004)	1430 (69%)		496 (24%)			9 (0.4%)	55 (2.6%)	61 (2.9%)	2073
Miller et al. (2004)	517 (51%)		43 (4.2%)	163 (16%)	50 (4.9%)	53 (5.2%)		148 (15%)	1019

visible albedo reduction of a snow surface (Warren and Wiscombe, 1980; Aoki et al., 2003). The relatively significant influence over the Arctic suggests that East Asian dust may exert greater climatic impact through those effects.

### 3.4. Comparison with other global dust model studies

Table 2 compares the regional annual dust flux of this and other recent global dust model studies (Werner et al., 2002; Luo et al., 2003; Zender et al., 2003a; Ginoux et al., 2004; Miller et al., 2004). While all studies agree that North Africa is the most important source region (more than 50%), they differ in the relative importance of other regions. Our model calculation indicates that 11% of global dust is emitted from East Asia, while other models indicate less than 5%. This study and those of Zender et al. (2003a) and Ginoux et al. (2004) calculated very small amounts of dust for North America (0.1%, 0.4%, and 0.5%), whereas Miller et al. (2004) calculated a relatively significant amount of 5.2%, which is greater than the calculated amount from the Arabian Peninsula or East Asia. Similar differences were found for Australian dust. However, no observational data are available to confirm the relative strengths of different source regions.

### 3.5. Case study: Dust deposition at Greenland

Biscaye et al. (1997) and Bory et al. (2002, 2003) reported that isotopic and mineralogical analyses indicate that the dust deposited on Greenland's ice core originates from East Asia. Their analyses reveal

the importance of long-range transport of Asian dust and provide a basis for evaluation of the dust model. Fig. 8 depicts the simulated total dust deposition flux at NorthGRIP (75.1°N, 42.3°W) in Greenland. The simulation shows that dust from eastern and western China is deposited on Greenland. However, a considerable amount of dust from North Africa, and occasionally from the Arabian Peninsula, is also deposited on the site. The estimated contributions from the various dust sources are as follows: 54% of the dust deposition on NorthGRIP comes from North Africa, 32% from East Asia (26% from eastern, and 6% from western China), 6% from the Middle East, and 5% from Central Asia.

Our model may have underestimated the source strength or northward transport of dust from East Asia or overestimated the source strength of North Africa, given that isotopic analyses of the dust deposition in Greenland indicate East Asian prevalence (Bory et al., 2003). Similar results have been reported in previous global modeling studies. Luo et al. (2003) reported that about 50% of the dust in Greenland is of North African origin; Werner et al. (2002) indicated that only about 30% of the dust in Greenland is from East Asia, according to their 'modern' simulation. The estimated dust emission from Asia in the previous studies was no greater than that in ours (Table 2), and thus it can be concluded that underestimation of the Asian dust influence on Greenland is a common problem with global dust transport models.

The contribution of the Taklimakan desert (western China) was simulated to be particularly small in our model. The probable cause for this discrepancy between the observation and simulation is the coarse resolution

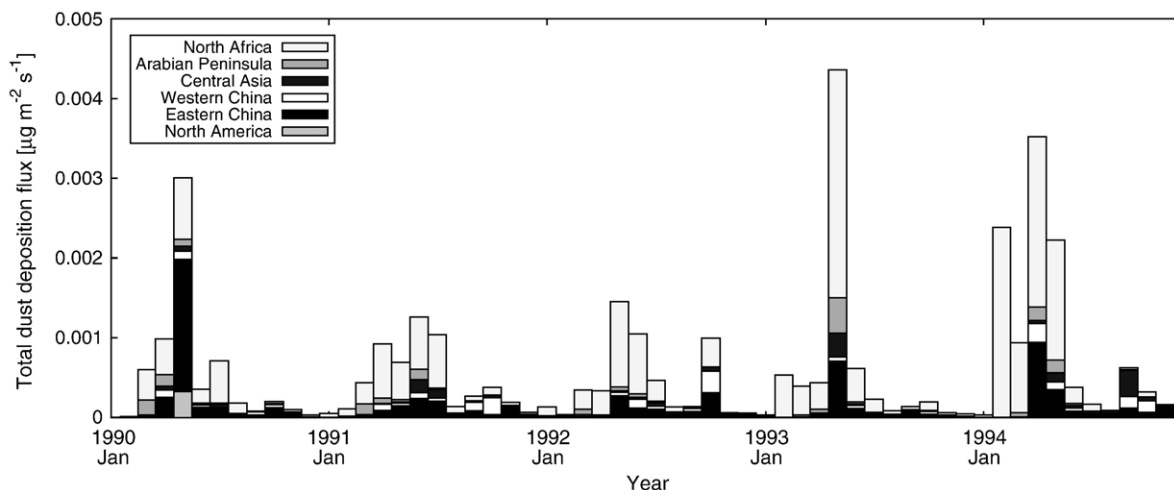


Fig. 8. Temporal variation of the simulated monthly averaged total deposition flux at NorthGRIP (75.1°N, 42.3°W, Greenland). The contributions of various source regions are illustrated in colors. Contributions from the source regions in the southern hemisphere were negligible.

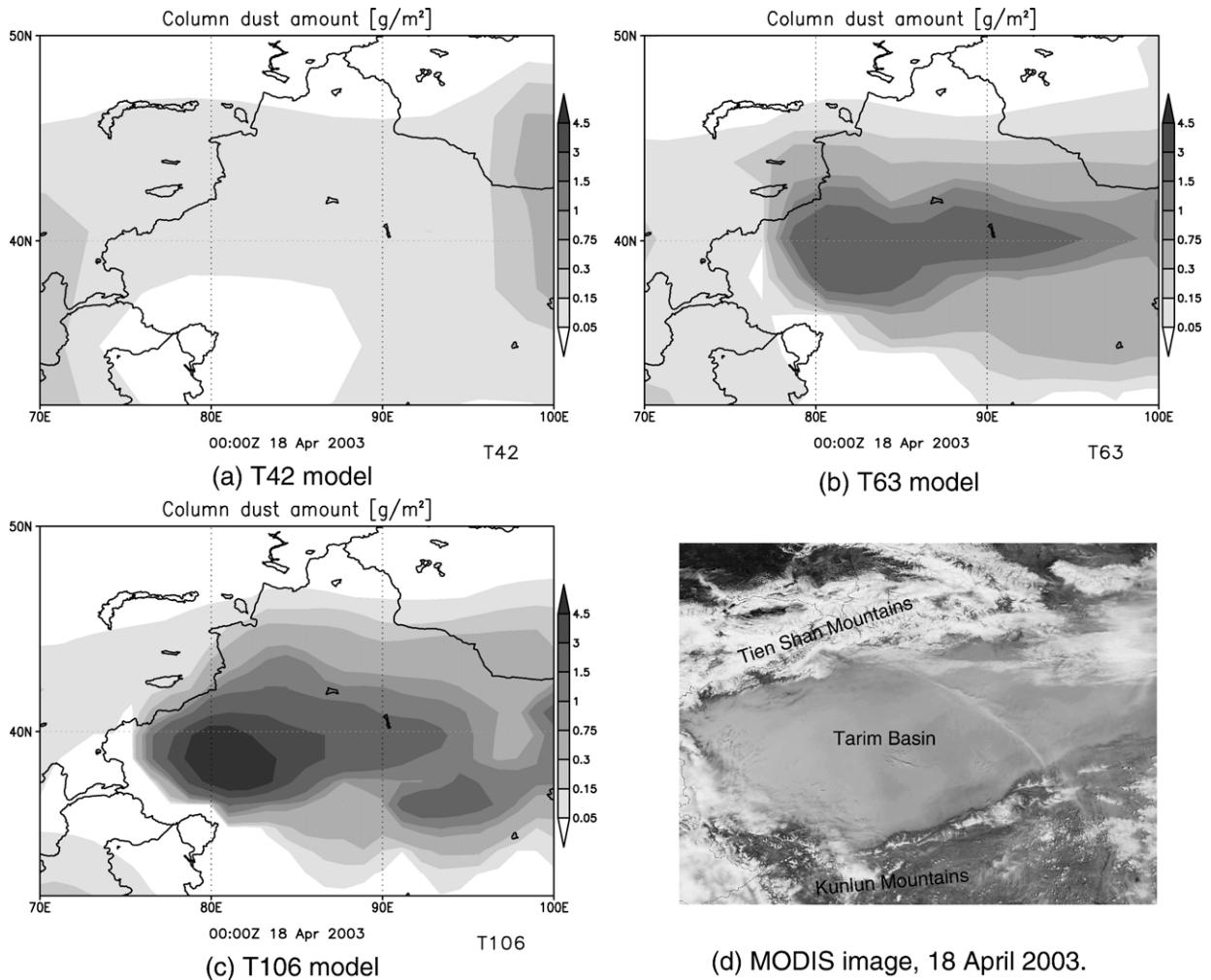


Fig. 9. Simulated column integrated dust mass on 18 April 2003 with horizontal resolutions of (a) T42, (b) T63, and (c) T106. The true-color image taken by the Moderate Resolution Imaging Spectroradiometer (MODIS) on NASA's Aqua satellite is also provided in (d). The MODIS image is taken from NASA's Earth Observatory (<http://earthobservatory.nasa.gov/NaturalHazards>).

of the global model, which leads to inadequate representation of the complex topography of the Tarim Basin. Fig. 9 is an example of the differences in simulated dust at horizontal resolutions of T106 (about  $1.1^\circ$ ), T63 (about  $1.9^\circ$ ), and T42 (about  $2.8^\circ$ ). A dust storm blew over the Taklimakan desert on 19 April 2003, as indicated by the true-color image from the Moderate Resolution Imaging Spectroradiometer (MODIS) on NASA's Aqua satellite (Fig. 9d). While the T106 model predicted a strong dust storm over the Taklimakan desert, the T63 model predicted a weak dust storm, and the T42 model failed to predict the dust storm. There are two main causes for the differences; one is the representation of local circulation caused by the topography, and the other is an error in simulated

snow coverage and excessive soil moisture due to the melting of snow. In this particular case, the T42 model failed to reproduce the topographic local winds caused by the Tarim Basin. This example demonstrates that simulated dust in the Taklimakan desert is sensitive to topographical representation. It will be necessary to parameterize small-scale circulations since the T106 horizontal resolution is still too coarse to express the steep topography of the Tarim Basin. A recent study by Cakmur et al. (2004) incorporated a probability distribution of wind speed within a grid box that depended on the wind speed explicitly calculated by the GCM. It would be beneficial to incorporate such a technique to account for topographically localized circulations. Simulations of the Taklimakan dust with

higher grid resolution by regional dust models (Liu et al., 2003; Uno et al., 2005) would also be beneficial to quantify the source strength of the region.

#### 4. Conclusion

We investigated the contributions of potential dust source regions using a numerical simulation with a global dust transport model, MASINGAR. The land area was divided into nine potential dust source regions: North and South Africa, the Arabian Peninsula, Central Asia, eastern and western China, North and South America, and Australia. The dust budgets and distributions of the source regions were presented. Dust originating from the Sahara Desert accounts for about 58% of the total dust emission and about 62% of the total dust load in the atmosphere. The Saharan dust significantly controls the dust distribution, not only over the Atlantic Ocean but also in most parts of the northern hemisphere. Australian dust dominates in the southern hemisphere. However, a comparison with the surface dust concentration suggested that the contribution of Saharan dust may have been overestimated by this model.

The emission and atmospheric load of dust from East Asia (eastern and western China) were estimated to be about  $214 \text{ Tg yr}^{-1}$  and  $1.1 \text{ Tg}$ , which account for about 11% and 6% of the total dust emission and the total atmospheric load. Dust originating from East Asia dominates the atmospheric load in the Asian Pacific region, at about 70% over China and Mongolia, 60% over Korea, 50% over Japan, and 40% over the North Pacific Ocean. Dust originating from regions other than East Asia, particularly from the Sahara, may also affect the Asian Pacific region.

The simulated total dust deposition at NorthGRIP (Greenland) revealed the influence of East Asian dust at the site. However, North African dust was found to be the foremost contributor to the dust deposition there. This finding contradicts the result of the isotopic analysis of Bory et al. (2003). This disagreement suggests that our model may have underestimated the dust emission from the Taklimakan desert or overestimated the influence of the Saharan dust. Insufficient representations of local wind and snow coverage due to the coarse horizontal resolution of the global dust model are possible causes of the underestimation of dust emission from the Taklimakan desert.

The results of this study are based only on a six-year simulation, which may not be sufficient to obtain the climatological state since the year-to-year variability of dust is significant. A more long-term integration will be necessary to obtain the climatological state. It is also

necessary to investigate the annual variability for the dust source region.

More observations to characterize dust particles would help clarify the contributions of the various dust source regions. These would include mineralogical, isotopic, and morphological analyses of airborne or deposited dust particles. A combination of the numerical experiment presented here and those observations would lead to reduced uncertainties in quantitative estimations of mineral dust aerosol.

#### Acknowledgments

We acknowledge that comments from the two anonymous reviewers are helpful for improving the original manuscript. We thank Drs. Masao Mikami and Yasunori Kurosaki of the Meteorological Research Institute for providing useful comments on this work. We are grateful to the Climate Research Department of the Meteorological Research Institute for the development of the MRI/JMA 98 GCM. We express our thanks to Prof. Joseph M. Prospero and Prof. Dennis L. Savoie for providing the University of Miami aerosol network data, and the British Atmospheric Data Centre for the HadISST data. This study was supported by the Cooperative System for Supporting Priority Research of the Japan Science and Technology Corporation.

#### References

- Aoki, T., Hachikubo, A., Hori, M., 2003. Effects of snow physical parameters on shortwave broadband albedos. *J. Geophys. Res.* 108 (D19), 4616. doi:10.1029/2003JD003506.
- Aoki, T., Tanaka, T.Y., Uchiyama, A., Chiba, M., Mikami, M., Key, J.R., 2005. Sensitivity experiments of direct radiative forcing by mineral dust using spectrally detailed radiative transfer model. *J. Meteorol. Soc. Jpn.* 83A, 315–331.
- Arakawa, A., Schubert, W.H., 1974. Interaction of a cumulus ensemble with the large-scale environment, part I. *J. Atmos. Sci.* 31, 674–701 (Apr.).
- Archer, D., Winguth, A., Lea, D., Mahowald, N., 2000. What caused the glacial/interglacial atmospheric  $\text{pCO}_2$  cycles? *Rev. Geophys.* 38 (2), 159–189.
- Biscaye, P.E., Grousset, F.E., Revel, M., der Gaast, S.V., Zielinski, G.A., Vaars, A., Kukla, G., 1997. Asian provenance of glacial dust (stage 2) in the Greenland Ice Sheet Project 2 Ice Core, Summit, Greenland. *J. Geophys. Res.* 102 (C12), 26765–26781.
- Bory, A.J.-M., Biscaye, P.E., Svensson, A., Grousset, F.E., 2002. Seasonal variability in the origin of recent atmospheric mineral dust at NorthGRIP, Greenland. *Earth Planet. Sci. Lett.* 196, 123–134.
- Bory, A.J.-M., Biscaye, P.E., Grousset, F.E., 2003. Two distinct seasonal Asian source regions for mineral dust deposited in Greenland (NorthGRIP). *Geophys. Res. Lett.* 30 (4), 1167. doi:10.1029/2002GL016446.
- Cakmur, R.V., Miller, R.L., Torres, O., 2004. Incorporating the effect of small-scale circulations upon dust emission in an atmospheric

- general circulation model. *J. Geophys. Res.* 109, D07201. doi:10.1029/2003JD004067.
- DeFries, R.S., Townshend, J.R.G., 1994. NDVI-derived land cover classification at a global scale. *Int. J. Remote Sens.* 15 (17), 3567–3586.
- Dentener, F.J., Carmichael, G.R., Zhang, Y., Lelieveld, J., Crutzen, P.J., 1996. Role of mineral dust aerosol as a reactive surface in the global troposphere. *J. Geophys. Res.* 101 (D17), 22869–22889.
- Dickerson, R.R., Kondragunta, S., Stenchikov, G., Civerolo, K.L., Doddridge, B.G., Holben, B., 1997. The impact of aerosols on solar UV radiation and photochemical smog. *Science* 278, 827–830.
- Dubovik, O., Holben, B., Eck, T.F., Smirnov, A., Kaufman, Y.J., King, M.D., Tanré, D., Slutsker, I., 2002. Variability of absorption and optical properties of key aerosol types observed in worldwide locations. *J. Atmos. Sci.* 59, 590–608.
- Duce, R.A., Unni, C.K., Ray, B.J., Prospero, J.M., Merrill, J.T., 1980. Long-range atmospheric transport of soil dust from Asia to the tropical north pacific: temporal variability. *Science* 29, 1522–1524.
- Fécan, F., Marticorena, B., Bergametti, G., 1999. Parameterization of the increase of the aeolian erosion threshold wind friction velocity due to soil moisture for arid and semi-arid areas. *Annales Geophysicae* 17, 149–157.
- Ginoux, P., Chin, M., Tegen, I., Prospero, J.M., Holben, B., Dubovik, O., Lin, S.-J., 2001. Sources and distributions of dust aerosols simulated with the GOCART model. *J. Geophys. Res.* 106 (D17), 20255–20273.
- Ginoux, P., Prospero, J.M., Torres, O., Chin, M., 2004. Long-term simulation of global dust distribution with the GOCART model: correlation with North Atlantic Oscillation. *Environ. Model. Softw.* 19, 113–128.
- Giorgi, F., Chameides, W.L., 1986. Rainout lifetimes of highly soluble aerosols and gases as inferred from simulations with a general circulation model. *J. Geophys. Res.* 91 (D13), 14367–14376.
- Goudie, A.S., Middleton, N.J., 1992. The changing frequency of dust storms through time. *Clim. Change* 20, 197–225.
- Grousset, F.E., Ginoux, P., Bory, A., Biscaye, P.E., 2003. Case study of a Chinese dust plume reaching the French Alps. *Geophys. Res. Lett.* 30 (6), 1277. doi:10.1029/2002GL016833.
- Husar, R.B., Tratt, D.M., Schichtel, B.A., Falke, S.R., Li, F., Jaffe, D., Gassó, S., Gill, T., Laulainen, N.S., Lu, F., Reheis, M.C., Chun, Y., Westphal, D., Holben, B.N., Gueymard, C., McKendry, I., Kuring, N., Feldman, G.C., McClain, C., Frouin, R.J., Merrill, J., DuBois, D., Vignola, F., Murayama, T., Nickovic, S., Wilson, W.E., Sassen, K., Sugimoto, N., Malm, W.C., 2001. The Asian dust of April 1998. *J. Geophys. Res.* 106 (D16), 18317–18330.
- Kanamitsu, M., Ebisuzaki, W., Woollen, J., Yang, S.-K., Hnilo, J.J., Fiorino, M., Potter, G.L., 2002. NCEP–DOE AMIP-II reanalysis (R-2). *BAMS* 83 (11), 1631–1643.
- Kubilya, N., Cokacar, T., Oğuz, T., 2003. Optical properties of mineral dust outbreaks over the northeastern Mediterranean. *J. Geophys. Res.* 108 (D21), 4666. doi:10.1029/2003JD003798.
- Kurosaki, Y., Mikami, M., 2005. Regional difference in the characteristics of dust event in East Asia: relationship among dust outbreak, surface wind, and land surface condition. *J. Meteorol. Soc. Jpn.* 83A, 1–18.
- Liu, M., Westphal, D.L., Wang, S., Shimizu, A., Sugimoto, N., Zhou, J., Chen, Y., 2003. A high-resolution numerical study of the Asian dust storms of April 2001. *J. Geophys. Res.* 108 (D23), 8653. doi:10.1029/2002JD003178.
- Lunt, D.J., Valdes, P.J., 2002. The modern dust cycle: comparison of model results with observations and study of sensitivities. *J. Geophys. Res.* 107 (D23), 4669. doi:10.1029/2002JD002316.
- Luo, C., Mahowald, N.M., del Corral, J., 2003. Sensitivity study of meteorological parameters on mineral aerosol mobilization, transport, and distribution. *J. Geophys. Res.* 108 (D15), 4447. doi: 10.1029/2003JD003483.
- Martin, J.H., 1991. Iron still comes from above. *Nature* 353, 123.
- Martin, J.H., Fitzwater, S.E., 1988. Iron-deficiency limits phytoplankton growth in the northeast Pacific subarctic. *Nature* 331 (6154), 341–343.
- Martin, R.V., Jacob, D.J., Yantosca, R.M., Chin, M., Ginoux, P., 2003. Global and regional decreases in tropospheric oxidants from photochemical effects of aerosols. *J. Geophys. Res.* 108 (D3), 4097. doi:10.1029/2002JD002622.
- McKendry, I.G., Hacker, J.P., Stull, R., Sakiyama, S., Mignacca, D., Reid, K., 2001. Long-range transport of Asian dust to the Lower Fraser Valley, British Columbia, Canada. *J. Geophys. Res.* 106 (D16), 18361–18370.
- Mellor, G.L., Yamada, T., 1974. A hierarchy of turbulence closure models for planetary boundary layers. *J. Atmos. Sci.* 31, 1791–1806.
- Miller, R.L., Tegen, I., Perlwitz, J., 2004. Surface radiative forcing by soil dust aerosols and the hydrologic cycle. *J. Geophys. Res.* 109 (D4), D04203. doi:10.1029/2003JD004085.
- Myhre, G., Stordal, F., 2001. Global sensitivity experiments of the radiative forcing due to mineral aerosols. *J. Geophys. Res.* 106 (D16), 18193–18204.
- Owen, P.R., 1964. Saltation of uniform grains in air. *J. Fluid Mech.* 20 (2), 225–242.
- Park, C.B., Sugimoto, N., Matsui, I., Shmizu, A., Tatarov, B., Kamei, A., Lee, C.H., Uno, I., Takemura, T., Westphal, D.L., 2005. Long-range transport of Saharan dust to east Asia observed with lidars. *SOLA* 1, 121–124.
- Penner, J.E., Andreae, M., Annegarn, H., Barrie, L., Feichter, J., Hegg, D., Jayaraman, A., Leaitch, R., Murphy, D., Nganga, J., Pitari, G., 2001. Aerosols: their direct and indirect effects. In: Houghton, J.T., Ding, Y., Griggs, D., Noguera, M., van der Linden, P.J., Dai, X., Maskell, K., Johnson, C.A. (Eds.), *Climate Change 2001: the Scientific Basis, Contribution of Working Group I to the Third Assessment Report of the Intergovernmental Panel on Climate Change*. Cambridge Univ. Press, New York, pp. 289–348. Ch. 5.
- Prospero, J., 1999. Long-term measurements of the transport of African mineral dust to the southeastern United States: implications for regional air quality. *J. Geophys. Res.* 104 (D13), 15917–15927.
- Prospero, J.M., Ginoux, P., Torres, O., Nicholson, S.E., Gill, T.E., 2002. Environmental characterization of global sources of atmospheric soil dust identified with the Nimbus 7 total ozone mapping spectrometer (TOMS) absorbing aerosol product. *Rev. Geophys.* 40 (1). doi:10.1029/2000RG000095.
- Pye, K., 1987. *Aeolian Dust and Dust Deposits*. Academic Press.
- Seinfeld, J.H., Pandis, S.N., 1997. *Atmospheric Chemistry and Physics: From Air Pollution to Climate Change*. A Wiley-Interscience Publication.
- Shao, Y., 2000. *Physics and Modelling of Wind Erosion*. Vol. 23 of Atmospheric and Oceanographic Sciences Library. Kluwer Academic Press, Dordrecht, the Netherlands.
- Shao, Y., Lu, H., 2000. A simple expression for wind erosion threshold friction velocity. *J. Geophys. Res.* 105 (D17), 22437–22443.
- Shao, Y., Raupach, M.R., Leys, J.F., 1996. A model for predicting aeolian sand drift and dust entrainment on scales from paddock to region. *Aust. J. Soil Res.* 34, 309–342.
- Shibata, K., Yoshimura, H., Ohizumi, M., Hosaka, M., Sugi, M., 1999. A simulation of troposphere, stratosphere and mesosphere with an MRI/JMA98 GCM. *Pap. Meteorol. Geophys.* 50, 15–53.

- Sokolik, I.N., Toon, O.B., 1996. Direct radiative forcing by anthropogenic airborne mineral aerosols. *Nature* 381, 681–683.
- Tanaka, T.Y., Chiba, M., 2005. Global simulation of dust aerosol with a chemical transport model, MASINGAR. *J. Meteorol. Soc. Jpn.* 83A, 255–278.
- Tanaka, T.Y., Orito, K., Sekiyama, T.T., Shibata, K., Chiba, M., Tanaka, H., 2003. MASINGAR, a global tropospheric aerosol chemical transport model coupled with MRI/JMA98 GCM: model description. *Pap. Meteorol. Geophys.* 53 (4), 119–138.
- Tanaka, T.Y., Kurosaki, Y., Chiba, M., Matsumura, T., Nagai, T., Yamazaki, A., Uchiyama, A., Tsunematsu, N., Kai, K., 2005. Possible transcontinental dust transport from North Africa and the Middle East to East Asia. *Atmos. Environ.* 39 (21), 3901–3909.
- Tazaki, K., Wakimoto, R., Minami, Y., Yamamoto, M., Miyata, K., Sato, K., Saji, I., Chaerun, S.K., Zhou, G., Morishita, T., Asada, R., Segawa, H., Imanishi, H., Kato, R., Otani, Y., Watanabe, T., 2004. Transport of carbon-bearing dusts from Iraq to Japan during Iraq's war. *Atmos. Environ.* 38 (14), 2091–2109.
- Tegen, I., Lacis, A.A., 1996. Modeling of particle size distribution and its influence on the radiative properties of mineral dust aerosol. *J. Geophys. Res.* 101 (D14), 19237–19244.
- Tegen, I., Harrison, S.P., Kohfeld, K., Prentice, I.C., Coe, M., Heimann, M., 2002. Impact of vegetation and preferential source areas on global dust aerosol: results from a model study. *J. Geophys. Res.* 107 (D21), 4576. doi:10.1029/2001JD000963.
- Uno, I., Harada, K., Satake, S., Hara, Y., Wang, Z., 2005. Meteorological characteristics and dust distribution of the Tarim Basin simulated by the nesting RAMS/CFORS dust model. *J. Meteorol. Soc. Jpn.* 83A, 219–239.
- Warren, S.G., Wiscombe, W.J., 1980. A model for the spectral albedo of snow. II: Snow containing atmospheric aerosols. *J. Atmos. Sci.* 37 (12), 2734–2745.
- Webb, R.W., Rosenzweig, C.E., Levine, E.R., 2000. Global soil texture and derived water-holding capacities (Webb et al.). data set. Available on-line [<http://www.daac.ornl.gov>] from Oak Ridge National Laboratory Distributed Active Archive Center, Oak Ridge, Tennessee, U.S.A.
- Werner, M., Tegen, I., Harrison, S.P., Kohfeld, K.E., Prentice, I.C., Balkanski, Y., Rodhe, H., Roelandt, C., 2002. Seasonal and interannual variability of the mineral dust cycle under present and glacial climate conditions. *J. Geophys. Res.* 107 (D24), 4744. doi:10.1029/2002JD002365.
- Wilson, M., Henderson-Sellers, A., 1985. A global archive of land cover and soils data for use in general circulation climate models. *J. Climatol.* 5, 119–143.
- Zender, C.S., Bian, H., Newman, D., 2003a. Mineral Dust Entrainment and Deposition (DEAD) model: description and 1990s dust climatology. *J. Geophys. Res.* 108 (D14), 4416. doi:10.1029/2002JD002775.
- Zender, C.S., Newman, D., Torres, O., 2003b. Spatial heterogeneity in aeolian erodibility: uniform, topographic, geomorphic, and hydrologic hypotheses. *J. Geophys. Res.* 108 (D17), 4543. doi:10.1029/2002JD003039.
- Zender, C.S., Miller, R.L., Tegen, I., 2004. Quantifying mineral dust mass budgets: terminology, constraints, and current estimates. *Eos* 85 (48), 509–512. doi:10.1029/2004EO480002.
- Zobler, L., 1986. A world soil file for global climate modeling. NASA Tech. Memo. 87802, NASA. 33 pp.